Part-level Car Parsing and Reconstruction from Single Street View

Qichuan Geng^{1,2}, Feixiang Lu^{1,2}, Xinyu Huang^{2,4}, Sen Wang³, Xinjing Cheng^{2,4}, Zhong Zhou¹, and Ruigang Yang^{2,4}

Beihang University, Beijing, China¹
Baidu Research, Beijing, China²
Northwestern Polytechnical University, Xi'an, China³
National Engineering Laboratory of Deep Learning Technology and Application, China⁴
{gengqichuan, lufeixiang, huangxinyu01, chengxinjing, yangruigang}@baidu.com
{zhaokefirst, flylu, zz}@buaa.edu.cn, wangsen1312@gmail.com

Abstract

In this paper, we make the first attempt to build a framework to simultaneously estimate semantic parts, shape, translation, and orientation of cars from single street view. Our framework contains three major contributions. Firstly, a novel domain adaptation approach based on the class consistency loss is developed to transfer our part segmentation model from the synthesized images to the real images. Secondly, we propose a novel network structure that leverages part-level features from street views and 3D losses for pose and shape estimation. Thirdly, we construct a high quality dataset that contains more than 300 different car models with physical dimensions and part-level annotations based on global and local deformations. We have conducted experiments on both synthesized data and real images [13]. Our results show that the domain adaptation approach can bring 35.5 percentage point performance improvement in terms of mean intersection-over-union score (mIoU) comparing with the baseline network using domain randomization only. Our network for translation and orientation estimation achieves competitive performance on highly complex street views (e.g., 11 cars per image on average). Moreover, our network is able to reconstruct a list of 3D car models with part-level details from street views, which could benefit various applications such as finegrained car recognition, vehicle re-identification, and traffic simulation.

1. Introduction

Global features that are extracted from colors, textures, and contours, of an image or an object instance are important for learning image or object structure. However, they cannot handle well with partial occlusions, large viewpoint

variations, or deformations. On the other hand, semantic parts could provide us additional and useful information in various vision tasks. For instance, part-based models have been applied in fine-grain recognition [12, 38, 35], object detection and segmentation [34, 5], human pose estimation [33, 10], and face parsing [19, 14, 27]. However, we found that there is very limited research has been done in part-level car parsing, which could benefit applications such as autonomous driving, fine-grained car recognition, vehicle re-identification, and car damage assessment. Currently, one dominant research direction is to estimate 3D car poses from detected key points that could be considered as a compact representation of car semantic parts [39, 23]. However, precise key point localization could still be a hard problem even for frontal faces [7]. Inaccurate detections caused by changing viewpoints, lighting conditions, and occlusions could greatly affect the reconstruction quality. More importantly, key points for cars are often not well defined. For example, car lights could have quite different shapes even for the same car model with different years. Therefore, car lights may not be well localized by four key points as defined in [39, 18] and one key point defined in [2]. Another promising direction is to apply the approximate differentiable renderer [21] to render the 3D car models and then compare the projections with the instance masks and/or depth maps, such as the render-to-compare loss proposed in [15]. However, we found that even a projection that is matched with ground truth instance mask or depth map could still contain certain pose confusions that could be further aggravated when partial occlusions present. When depth maps are not available and arbitrary measurement units are used in CAD models, 3D reconstruction problem itself is ill-posed from a single view.

In this paper, we make the first attempt to build a framework to simultaneously estimate semantic parts, shape, translation, and orientation of cars from single street view. There are three major contributions:

- We propose a deep network to segment car parts in street views and transfer the model from synthesized data to real images. As domain randomization is not enough to reduce the gap, we develop a novel domain adaptation approach based on the class consistency loss.
- We propose a novel network for 3D pose and shape estimation. This network integrates global and local part features and directly minimizes the losses such as car center translation and per-vertex geometric errors.
- 3. We build a high quality dataset that contains 348 car models with part-level annotations and physical dimensions. We apply global and local deformations to build dense correspondences among point clouds so that we can transfer textures and part annotations across these models. Both our 3D dataset and 2D synthesized images will be made public.

2. Related Work

In this section, we discuss two related research areas. The first is the usage of semantic parts for solving vision-based tasks. The second is the estimation of car pose and/or shape from single image.

Semantic Parts These semantic parts could be represented by key points, rectangles, and regions. As it is very time consuming to annotate regions at pixel-level, key points and rectangles could be considered as compact representations and are commonly used in many tasks. In this paper, we mainly focus on the regions annotated at pixel-level that have been emerged in recent years. In [33], Varol et al. proposed the SURREAL dataset (synthetic humans for real tasks) that contains synthetic 2D/3D human poses, depth maps, part segments, and normal maps. A stacked hourglass network is adopted to segment 14 human parts. Liang et al. proposed a local-global long short-term memory architecture for clothes segmentation in [17]. In [5], Chen et al. provided a new dataset with annotated body parts of animals in PASCAL VOC 2010 [8]. A network is proposed so that body parts could be ignored when they cannot be reliably detected. Liu et al. further extend the PASCAL dataset to the PASCAL semantic part dataset (PASPart) that have part-level annotations of 20 categories [20]. In [28], Song et al. propose a 2-stream FCN network to extract 3D geometric features to segment car parts in the PASPart dataset. Although there are few hundreds images containing cars in the dataset, there are two major differences comparing with our 2D and 3D datasets. Firstly, each car image in PAS-CAL contains very limited number of cars (e.g., one car per image) with large resolutions, which make the dataset unsuitable for the autonomous driving application. Second,

there are only 2D parts annotated in the PASPart while 3D poses and shapes are not available.

Semantic parts could be easily generated for human faces based on facial landmarks and contours and used for face parsing algorithms [19, 14, 27]. However, Smith et al. claimed that most landmarks are not well-defined [27]. Moreover, it is unclear how many landmarks should be used and it is difficult to measure location uncertainties caused by human labelers.

Car Pose and Shape Estimation Car pose estimation, especially in 3D space, could be considered as one of the most important tasks for applications like autonomous driving, fine-grained categorization, and car damage assessment. Pose estimation could be done by using point clouds scanned by LiDAR sensors, single or multiple image frames, and fusion of these two modalities. In this paper, we focus on the 3D pose estimation using single street view.

In [40], Zhu et al. trained a set of 2D part descriptors corresponding to selected 3D landmarks. These part descriptors are used to estimate 3D car shapes based on global geometric consistency. Zhou et al. proposed a convex relaxation approach to estimate 3D shape given a set of 2D key points [39] and a stacked hourglass network to localize these semantic key points [23]. Wang et al. proposed a network framework for 3D pose estimation with the purpose of fine-grained car categorization [34]. Fine-grained 3D pose datasets for cars are built that contain 2D images and 3D models. Poirson et al. propose a network for detection rough pose estimation from single shot without using parts or initial bounding boxes [24]. Su et al. proposed an image synthesis pipeline and deep networks for viewpoint estimation [30]. We found that many existing networks are designed for pose estimation of general objects. Although car is often one of these objects, cars in most images are clear, non-occluded, and have relatively large resolutions that could be quite different from cars captured in street views.

The research on car pose and/or shape estimation from single street views is still limited [4, 22, 2, 37, 15]. In [4], Chen et al. sample candidate bounding boxes in the 3D space and use labeled class/instance semantic, contour, shape, location, and so on as prior to score the candidate boxes. Mousavian proposed two deep networks for 3D bounding box estimation [22]. One network estimates 3D orientation based on a discrete-continuous loss and another network regresses the 3D dimensions. Chabot et al. [2] proposed a deep MANTA network to estimate 3D vehicle model. The model is built by a wire-frame skeleton based on the pre-defined 3D landmarks. The car parts are then represented by regions enclosed by the 3D landmarks. Xiang et al. proposed a novel representation, 3D voxel pattern, to encode appearance, shape, pose, and other properties [37].

The most related work is the 3D-RCNN network [15]

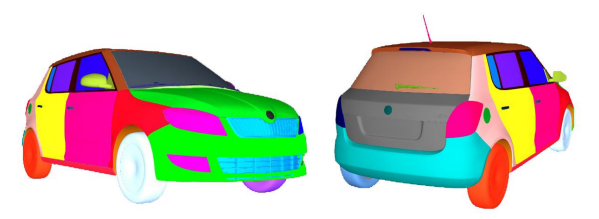


Figure 1. An example of 3D car model with part-level annotations

that estimates both 3D shapes and poses from single street view. The key innovation is a differentiable render-tocompare loss that allows supervision from 2D annotations. There are three major differences between 3D-RCNN and our work. Firstly, although 3D-RCNN estimates the azimuth angle and car shape, the 3D translation that could be the most key information in autonomous driving is not estimated. Secondly, semantic parts of cars are also not estimated in 3D-RCNN. In our framework, we use the part segmentation network to explicitly segment the car parts and transfer the network to the domain of real images. Thirdly, although both instance masks and depth maps could be used in the render-to-compare loss, there are only around 200 instance-level car masks provided in the Kitti dataset [9], which may not be sufficient to train a deep neural network with good performance. As a result, depth maps could provide a major contribution in the render-to-compare loss for the car pose and shape estimation. It remains unclear that the network could have the same performance when depth maps are not available. Instead of relying on a large set of depth maps, our network minimizes 3D losses based on our 3D car models.

3. Generation of 3D Car Models

In this section, we present our 3D car dataset and describe key steps for its generation. Our dataset has two unique characteristics comparing with many existing car datasets (e.g., ShapeNet [3] and synthesized datasets [26, 25]). Firstly, we annotate the 3D car models with semantic part information. We decompose each car into 70 exterior parts, from large parts such as front door and roof, to small parts such as door handle and car logo (Figure 1). Second, all the 3D car models in our dataset are accurately aligned with major physical dimensions including wheelbase, front/rear overhang, track width, overall width/height/length, and so on. Without physical dimensions, the 3D-RCNN network has to pre-assign a fixed scaling factor to normalized car models and further use depth maps to constraint the 3D object distances. Otherwise, the cars with different scaling factors may have very similar instance masks and 2D bounding boxes on different locations along the ray through the car center projection.

As it is labor-intensive to annotate 3D part information, we propose a procedure as shown in Figure 2 to transfer

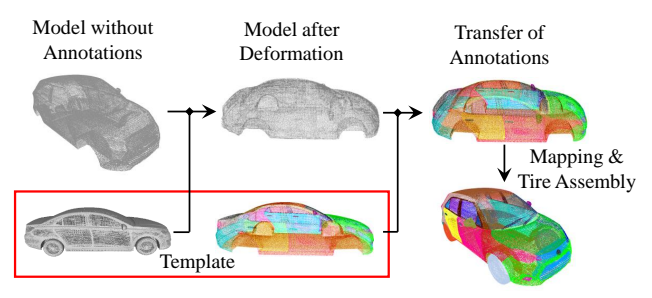


Figure 2. Illustration of procedure to build dense correspondences.

parts and textures from annotated models to un-annotated models and then further extend the dataset with more models so that the dataset could cover majority of car shapes on streets.

Template Selection We manually divide a large set of vehicles into categories based on vehicle geometries. For instance, we group most of cars, SUVs and minivans with four doors into one category and then select a common seen car as a template for this category. In fact, we find that any vehicle within the category could be served as the template and would not affect the remaining steps in this procedure.

Dense Correspondences We develop an algorithm to align each model in a category to the selected template. Most of car models are built with non-uniform mesh grids. Therefore, in our first step, we repair and re-mesh the car models so that point clouds are uniformly distributed with the pointto-point distance around one centimeter. Second, we apply a global alignment (i.e., iterative closest point [1]) to align two set of points clouds based on translation, rotation, and scaling operations. This is a rough alignment between two sets of point clouds. Third, we apply embedded deformation [31, 29] to construct the deformation graph and align the model with the template. After these three steps, we are able to build dense correspondences between the template and the point cloud of another model in the category. As a result, we are able to transfer part and texture information from 40 annotated models to more than 300 un-annotated models.

3D Shape Space We use PCA to find a $N \times 22$ dimensional shape basis for each category where N is the number of points of one car model. New car models can be generated by providing new 22 dimensional PCA parameters. Based on the procedure to estimate dense correspondence, we are also able to transfer part and texture information.

Notice that wheels and tires are processed separately as their shapes may not be well-maintained after rigid and non-rigid transformations. In order to maintain circular shapes after transformations, we only apply a scaling operation on wheels and tires. The diameters are estimated based on the shapes of transformed body fenders.

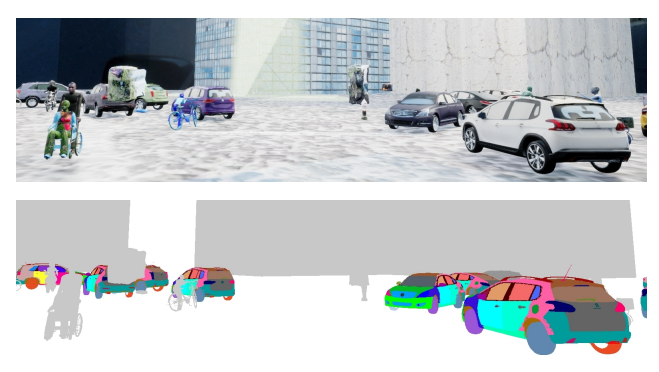


Figure 3. (*top*) An example of synthesized images with variations on lighting conditions, car models, textures, locations, and so on. (*bottom*) Corresponding annotations with 70 semantic parts.

4. Part-level Segmentation

Given our 3D models, it is possible to synthesize 2D image datasets with different purposes. In this paper, as we focus on the pose and shape estimation from single street view, we need to take a number of factors into consideration, such as illumination, occlusion, texture, and other related objects. We first adopt the domain randomization approach proposed in [32] to synthesize more than 60,000 images with sufficient variations on the above factors.

4.1. Domain Randomization

Specifically, we select a number of car models and other objects like pedestrians, cyclists, and traffic cones randomly from our 3D dataset. After applying collision detection, we randomly place them on the ground plane. Background image is selected from a large image collection that includes some background images cropped from real street views. We generate 5 to 20 lighting sources for each scene and place them in random locations with random orientations. Figure 3 shows an example of our rendered images and corresponding part-level annotations.

Domain randomization is an effective approach to bridge the reality gap. It has been shown that the AP score of car detector after fine-tuning on real images can be improved by 2.1% comparing with the detector trained on real data only [32]. However, for segmentation problem especially at the part-level, we cannot obtain decent segmentation performance on real images. In order to further reduce the domain gap, we propose a novel domain adaptation structure.

4.2. Domain Adaptation with Class Consistency

Experiments based on our synthesized data are conducted before we develop our domain adaptation approach. Firstly, we find that the feature encoder trained for a binary classifier for the car class cannot be used directly as the feature encoder for the classifier of parts. However, we find that a pixel that has been classified as one of parts is

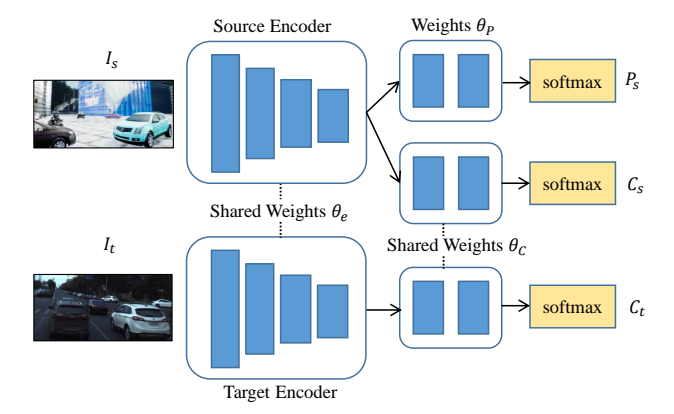


Figure 4. The network structure for domain adaptation.

likely classified as a car class. This tells us that the features learned at the part-level often can be used as the features at a higher hierarchical level, which is not true on the contrary.

Although we do not have part-level annotations on real images, we have real images annotated at a higher hierarchical level, i.e., class-level. The class-level annotations could be easily obtained from open datasets such as Cityscapes [6] and ApolloScape [13]. Therefore, we add a class consistency loss that bridges the differences between real data and simulated data.

Our network architecture for domain adaptation is given in Figure 4. We choose ResNet-38 network [36] as our backbone network, in which res5c output as the feature encoder. Let us denote I_s, I_t as the input images, C_s, C_t as class-level annotations in source (synthesized) domain and target (real) domain respectively, and P_s is the part-level annotations in the source domain. We minimize the loss:

$$L = L_{sp}(I_s, P_s; \theta_e, \theta_P) + \lambda_1 L_{sc}(I_s, C_s; \theta_e, \theta_C) + \lambda_2 L_{tc}(I_t, C_t; \theta_e, \theta_C)$$
(1)

where θ_e denotes the shared parameters of the feature encoder, θ_C and θ_P represent the parameters for class-level classifier and part-level classifier respectively, L_{sp} is the part-level loss in the source domain, and L_{sc} and L_{tc} are the class consistency losses in both source and target domains. λ_1 and λ_2 are the weights for L_{sc} and L_{tc} , which are set to 1s in our training stage.

5. Pose Estimation and Shape Reconstruction

The network architecture is shown in Figure 5. The Mask-RCNN network [11] is used as our backbone network. Both global features and part-level segmentation results are passed into the ROI feature extraction layer that outputs feature maps with fixed sizes. The ROI feature extraction layer is modified to record the original x and y coordinates of semantic parts. Instance mask, global features,

and part-level features are concatenated together as a final feature map with dimension $512\times14\times14$.

In [22], CNN regression is applied on 3D bounding box orientation and dimensions while the 3D translation is estimated in the post-processing step by the SVD decomposition. Similarly, in [2], 3D translation is also not estimated by the network and solved by the PnP algorithm [16] as a post-processing step. As mentioned in [15], it is fundamentally ill-posed to estimate 3D translation from cropped and resized ROI features. As a result, the loss based on amodal-box is proposed in [15]. As we have semantic parts and their x and y coordinates in the original image, and physical dimensions of 3D car models, we are able to design our network to estimate 3D translation directly.

The direct L_1 losses are given by

$$L_{direct} = \|\mathbf{c} - \mathbf{c}^*\|_{L_1} + \|\mathbf{s} - \mathbf{s}^*\|_{L_1} + \|\theta_b + \Delta\theta - \theta^*\|_{L_1} + \|\frac{1}{d_b + \Delta d} - \frac{1}{d^*}\|_{L_1}$$
(2)

In the first term, c and c* represent 2D projections of car centers from the network and ground truth respectively. The second term is the loss of 22 dimensional shape parameters where s is the network output and s* is the ground truth parameters. The third term and fourth term are the losses for pose angles and inverse depths of car centers. Similar to [15, 22], we apply classification first by dividing the parameter spaces into multiple bins and apply regression on each bin. θ_b in the third term is the average value in a bin, $\Delta\theta = \arctan\frac{\sin\Delta\theta}{\cos\Delta\theta}$ where $(\sin\Delta\theta,\cos\Delta\theta)$ are the network outputs representing the regressed values for each bin, and θ^* is the ground truth angles. $\theta = (\alpha, \beta, \gamma)$ represents the azimuth, elevation, and tilt angles. In the fourth term, d_b is the bin average depth, Δd is the regressed value for the bin, and d^* is the ground truth depth.

Different parameters, especially for shape and angle parameters, could have different effects on the final pose and shape estimation. Therefore, direct L_1 losses are not enough for pose and shape estimation. We propose the 3D losses that are given by

$$L_{3D} = \sum_{i=1}^{N} \|V_i - V_i^*\|_2 + \sum_{i=1}^{N} \|RV_i - R^*V_i^*\|_2 + \|R_c t - R_c^* t^*\|_2$$
(3)

where V_i and V_i^* represent the 3D coordinates of *i*-th estimated and ground truth vertex of the car model with N vertices. V_i is computed from the estimated shape parameters s and the PCA basis built from 348 car models.

 $R_c t = R_c [0,0,d_b+\Delta d]^T$ is the estimated 3D translation and $R_c^* t^* = R_c^* [0,0,d^*]^T$ is the ground truth 3D translation. Similar to the allocentric representation in [15], rotation matrix R is decomposed into $R_c R_v$ during the training where R_c is the rotation from the camera principal axis to the ray passing through the projection of car center c.

The loss from re-projection errors is given by

$$L_{reproj} = \sum_{i=1}^{N} \|p_i - p_i^*\|_2$$
 (4)

where p_i and p_i^* are the 2D projections of estimated car model and ground truth car model. L_{reproj} could be considered as the loss similar to the differentiable renderer. As our 3D losses play a major role in the network, L_{reproj} in our network is more like a re-weighting or attention mechanism that penalizes more on the cars close to the camera. The final loss is the weighted sum of L_{direct} , L_{3D} , and L_{reproj} .

6. Experiments

As our network aims to output more complete car information at the same time, it requires a more comprehensive dataset for training and testing. The Kitti dataset provides 3D information while around 200 instance-level masks may not be sufficient to train a deep network with good performance. The Cityscapes dataset contains 25,000 2D images with instance-level annotations, however, 3D information is not available. As a result, we choose the recent released ApolloScape dataset that contains both 3D information and 2D images with instance-level annotations [13]. We conduct following experiments to demonstrate superior performance of our work.

6.1. Part-level Segmentation

In the training stage, we randomly selected 5,000 synthesized images with part-level annotations and 5,000 images with car class-level annotations in the ApolloScape dataset. In order to evaluate our domain adaptation approach, we first select 1,700 synthesized images for testing. We further selected 200 images from the ApolloScape dataset as real testing images and manually annotate them at the partlevel. In these 200 real images, there are around 8 cars per image, and minimum and maximum car heights are 23 and 500 pixels respectively. We use the pre-trained model of the Resnet-38 network [36] and train our network end-to-end with 100 epochs with all parameters un-fixed. 13 semantic parts are used in training and testing, which are front light, front part, tail light, rear part, door, roof, roof rack, hood, mirror, side window, front window, rear window, and wheel/tire. The front part is a region including front bumper, front car logo, grilles and so on. Similarly, the rear part includes a set of parts in the rear region of a car.

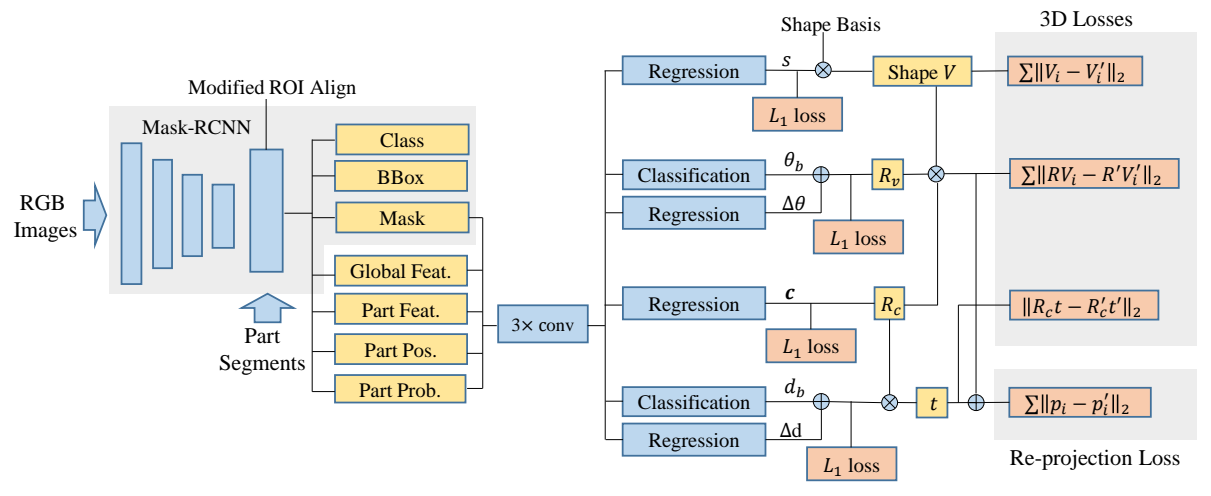


Figure 5. The network structure for estimation of translation, rotation, shape, and semantic parts in 3D space. Blue boxes represent network layers and modules, yellow boxes represent data entities, and orange boxes represent losses. Mask-RCNN [11] is used as backbone feature extractor. \oplus indicates the addition and \otimes indicates the multiplication.

The intersection-over-union scores (IoU) for individual parts are given in Table 1. When we train the network without using our domain adaptation approach, the parsing performance on real images is poor. One of possible reasons is that the lighting conditions on synthesized data and real images are still quite different, which enlarges the domain gap. Thus, domain randomization itself does not work well for part-level segmentation. With our domain adaptation approach, the segmentation performance (mIoU) can be improved by 35.5%. We illustrate some examples of our results in Figure 6. Notice that human labelers are unable to annotate some cars with small resolutions (e.g., the second and third columns in the Figure) and made mistakes on some small parts such as roof rack and mirror (e.g., the taxi in first column in the Figure) in the ground truth annotations while our transferred model segments them successfully.

We also observe that rear part, roof, and rear window have the highest IoUs (e.g., 0.739, 0.654, and 0.675) that are also close to the IoUs evaluated on synthesized data (e.g., 0.878, 0.753, and 0.859). The reason is that these three parts could be the parts with very high frequencies in the real domain. As a result, the domain knowledge for them can be easily transferred. This could be considered as a data imbalance problem that can be mitigated by re-weighting and re-sampling strategies.

In summary, to our knowledge, our work could be the first study of car part segmentation based on street views and we achieve very decent segmentation performance that can be used in practice.

6.2. Analysis of Part-level Features

During the training stage, we observe that almost all the losses except the L_1 loss of shape parameters are somewhat affected by part-level features. Figure 7 shows the

Table 1. The IoU scores for part-level parsing. The second and third columns are the results without using domain adaptation (DA) network structure. The fourth column contains results based on our domain adaptation structure.

mirror	0.719	0.033	0.404
hood	0.848	0.142	0.479
roof rack	0.862	0.034	0.174
door roof	0.869 0.753	0.080	0.523 0.654
rear part	0.878	0.173	0.739
tail light	0.815	0.184	0.359
front part	0.868	0.097	0.526
front light	0.781	0.082	0.251
train test	syn. syn.	syn. real	syn.+DA real

curves of L_1 pose angle loss. In the experiment, we train the pose and shape network with and without part-level features for 30 epochs. When part-level features are used, the pose loss drops quickly and then converges smoothly to near zero. However, without using part-level features, the pose loss converges to a certain value at a much slower speed. This proves that part-level features can effectively reduce the ambiguities caused by instance masks and instance features learned globally. This experiment could be considered as another evidence of our basic idea of designing the domain adaptation approach with class consistency loss (Sec-

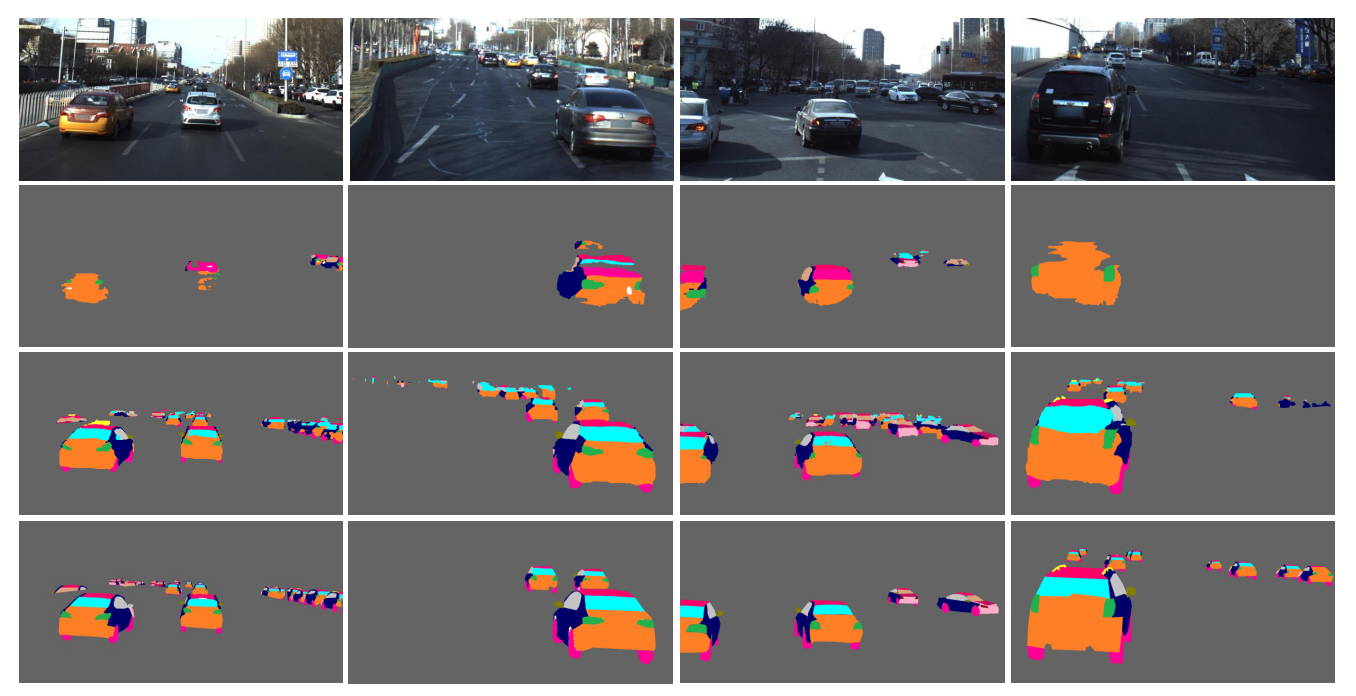


Figure 6. The examples of part parsing results. The first row contains the input images selected from ApolloScape dataset (cropped for visualization). The second row contains parsing results based on the domain randomization only. The third row contains results based on our domain adaptation structure. The fourth row contains the ground truth annotations.

tion 4.2). The fusion or concatenation of local features is likely to be used as the features for a classifier at a higher hierarchical level (e.g., instance mask, pose and so on). It may not be true on the contrary.

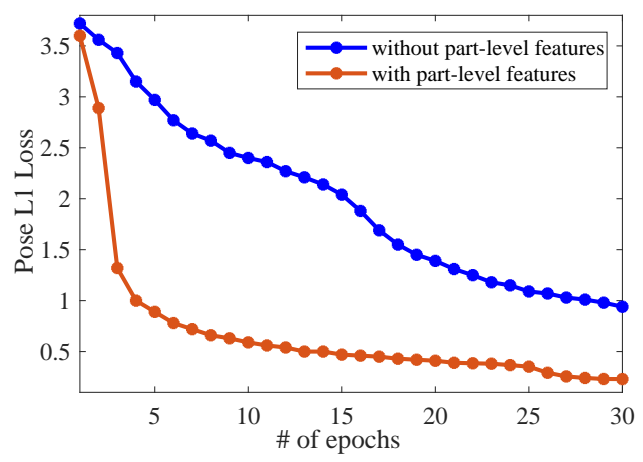


Figure 7. Analysis of part-level features on pose L_1 loss. The same network with and without part-level features are trained for 30 epochs.

6.3. Translation and Orientation Estimation

We train our pose and shape network with 4,236 image frames containing 3D car instances for 100 epochs and test the network on 1,041 images. Figure 8 shows some results

Table 2. Evaluation of 3D translation using mean distance error of car centers. [0,10) represents the distance ranging from 0 meter to 10 meters. The Deep3DBox is evaluated on all the difficulties including easy, moderate, and hard.

	MDE (meter)				
	[0,10)	[10,20)	[20,30)	[30,40)	[40,60)
Deep3DBox [22]	1.4	1.1	1.9	2.5	3.0
Our network	0.8	1.3	1.9	2.7	3.5

generated by our pose and shape network.

We evaluate 3D translation between car and camera separately as it is probably the most important car information in path planning in the area of autonomous driving. We adopt the evaluation metric in Deep3DBox, i.e., mean distance error for car centers (MDE). Table 2 compares the results between Deep3DBox and our network. Notice that 3D-RCNN network is not included in this comparison as 3D translation is not part of its outputs, and MDE results of Deep3DBox are estimated from Figure 8 in [22].

Average precision (AP) for detection and average orientation similarity (AOS) are adopted to evaluate car orientation. Table 3 shows the results for different approaches. The evaluation results of hard cases for 3D-RCNN, Deep3DBox, and Deep MANTA are listed in the table. Our network outputs all three pose angles while existing approaches only output the azimuth angle.

We would like to emphasize that it is difficult to pro-

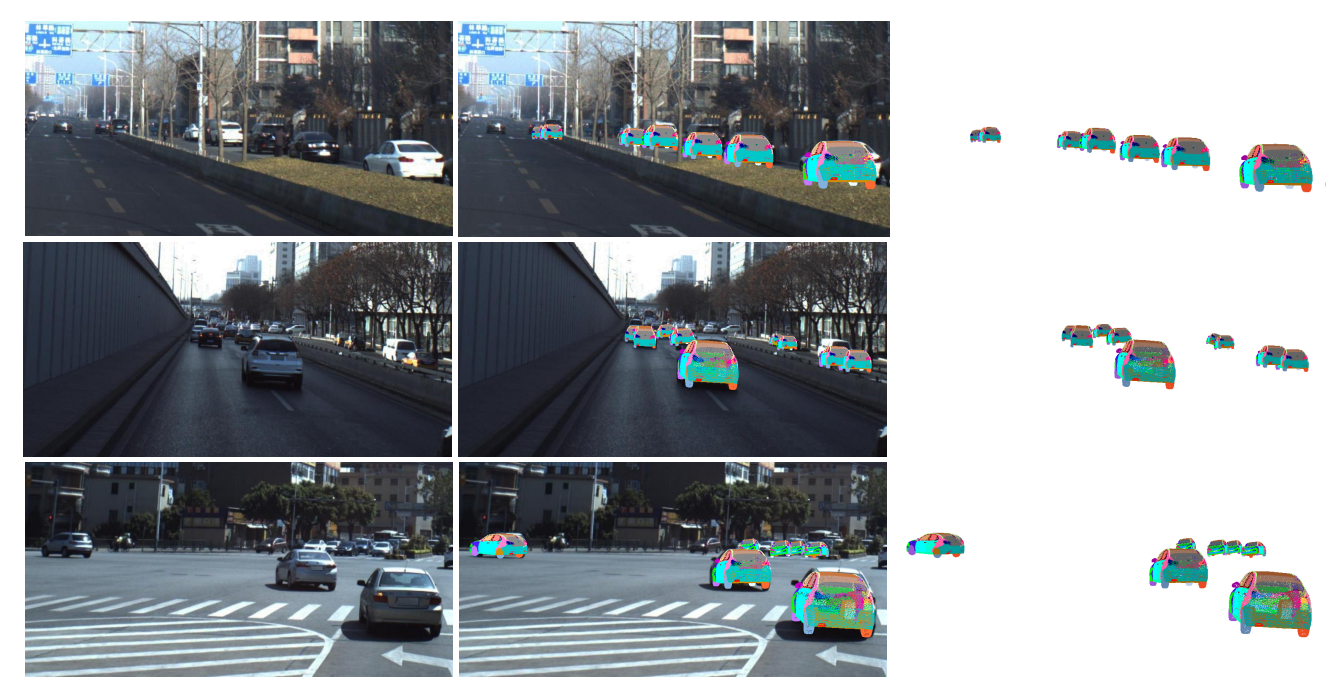


Figure 8. Examples of results generated by our network for pose estimation and shape reconstruction. The first column contains the original input images (cropped for visualization). The second column contains the overlay effects of the 3D models on the input images. The third column contains 3D car models with original 70 semantic parts.

Table 3. Evaluation of car orientation using average precision (AP) for detection and average orientation similarity (AOS). The results of hard cases for 3D-RCNN, Deep3DBox, and Deep MANTA are listed.

	Azimuth		Elevation	Tilt
	AP	AOS	AOS	AOS
3D-RCNN [15]	80.29%	80.07%	N/A	N/A
Deep MANTA [2]	80.79%	80.55%	N/A	N/A
Deep3DBox [22]	77.17%	76.76%	N/A	N/A
Our Network	79.58%	76.78%	78.77%	75.94%

vide a comparison at the same level based on two different datasets. Given that the ApolloScape dataset has a higher diversity and scene complexity, our network achieves very competitive results comparing with recently published approaches. For instance, there are 3.8 cars per image on average in the Kitti 7,481 training images. There are 11.1 cars per image on average in the 4,236 training images of the ApolloScape dataset. More cars in one image indicate more partial occlusions could present. Based on these statistics, the ApolloScape dataset could be more challenging even than the hard cases in the Kitti dataset. Figure 9 shows the distribution of number of cars per image for Kitti and ApolloScape training sets.

Notice that our pose and shape network not only outputs translation and orientation, but also reconstructs 3D car shapes that could be in the form of point clouds or triangle meshes along with 70 original semantic parts.

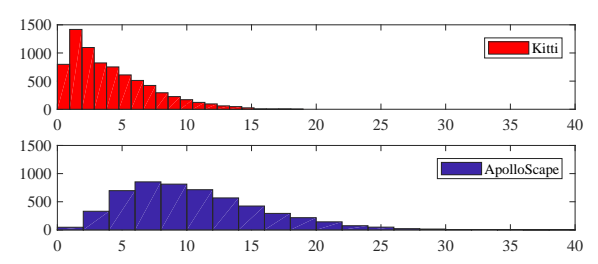


Figure 9. Distributions of number of cars per image for Kitti and ApolloScape datasets.

7. Conclusions and Future Works

In this work, we first propose a domain adaptation network structure to estimate semantic parts of cars. We then propose another network structure for pose and shape estimation. A high quality dataset of 3D car models with part-level annotations and physical dimensions is generated and will be released to public. Based on our dataset and network structures, we are the first to propose part-level car segmentation from single street view and our network framework is able to estimate more complete car information. We would like to explore two research directions in near future. Firstly, we plan to do more research to estimate and use part-level features for pose and shape estimation in an explicit and/or implicit manner. Second, we would like to apply similar network structure for different problems, such as fine-grained car recognition.

References

- [1] P. J. Besl and N. D. McKay. Method for registration of 3-d shapes. In Sensor Fusion IV: Control Paradigms and Data Structures, volume 1611, pages 586–607. International Society for Optics and Photonics, 1992. 3
- [2] F. Chabot, M. Chaouch, J. Rabarisoa, C. Teulière, and T. Chateau. Deep manta: A coarse-to-fine many-task network for joint 2d and 3d vehicle analysis from monocular image. In *Proc. IEEE Conf. Comput. Vis. Pattern Recog*nit.(CVPR), pages 2040–2049, 2017. 1, 2, 5, 8
- [3] A. X. Chang, T. Funkhouser, L. Guibas, P. Hanrahan, Q. Huang, Z. Li, S. Savarese, M. Savva, S. Song, H. Su, J. Xiao, L. Yi, and F. Yu. ShapeNet: An Information-Rich 3D Model Repository. Technical Report arXiv:1512.03012 [cs.GR], Stanford University — Princeton University — Toyota Technological Institute at Chicago, 2015. 3
- [4] X. Chen, K. Kundu, Z. Zhang, H. Ma, S. Fidler, and R. Urtasun. Monocular 3d object detection for autonomous driving. In *Proceedings of the IEEE Conference on Computer Vision and Pattern Recognition*, pages 2147–2156, 2016.
- [5] X. Chen, R. Mottaghi, X. Liu, S. Fidler, R. Urtasun, and A. Yuille. Detect what you can: Detecting and representing objects using holistic models and body parts. In *Proceedings of the IEEE Conference on Computer Vision and Pattern Recognition*, pages 1971–1978, 2014. 1, 2
- [6] M. Cordts, M. Omran, S. Ramos, T. Rehfeld, M. Enzweiler, R. Benenson, U. Franke, S. Roth, and B. Schiele. The cityscapes dataset for semantic urban scene understanding. In *Proceedings of the IEEE conference on computer vision* and pattern recognition, pages 3213–3223, 2016. 4
- [7] X. Dong, S.-I. Yu, X. Weng, S.-E. Wei, Y. Yang, and Y. Sheikh. Supervision-by-registration: An unsupervised approach to improve the precision of facial landmark detectors. In *Proceedings of the IEEE Conference on Computer Vision* and Pattern Recognition, pages 360–368, 2018. 1
- [8] M. Everingham, L. Van Gool, C. K. Williams, J. Winn, and A. Zisserman. The pascal visual object classes (voc) challenge. *International journal of computer vision*, 88(2):303– 338, 2010.
- [9] A. Geiger, P. Lenz, C. Stiller, and R. Urtasun. Vision meets robotics: The kitti dataset. *The International Journal of Robotics Research*, 32(11):1231–1237, 2013. 3
- [10] K. Gong, X. Liang, Y. Li, Y. Chen, M. Yang, and L. Lin. Instance-level human parsing via part grouping network. arXiv preprint arXiv:1808.00157, 2018. 1
- [11] K. He, G. Gkioxari, P. Dollár, and R. Girshick. Mask r-cnn. In Computer Vision (ICCV), 2017 IEEE International Conference on, pages 2980–2988. IEEE, 2017. 4, 6
- [12] S. Huang, Z. Xu, D. Tao, and Y. Zhang. Part-stacked cnn for fine-grained visual categorization. In *Proceedings of the IEEE Conference on Computer Vision and Pattern Recognition*, pages 1173–1182, 2016. 1
- [13] X. Huang, X. Cheng, Q. Geng, B. Cao, D. Zhou, P. Wang, Y. Lin, and R. Yang. The apolloscape dataset for autonomous driving. arXiv: 1803.06184, 2018. 1, 4, 5
- [14] M. M. Kalayeh, B. Gong, and M. Shah. Improving facial attribute prediction using semantic segmentation. In *Computer*

- Vision and Pattern Recognition (CVPR), 2017 IEEE Conference on, pages 4227–4235. IEEE, 2017. 1, 2
- [15] A. Kundu, Y. Li, and J. M. Rehg. 3d-rcnn: Instance-level 3d object reconstruction via render-and-compare. In Proceedings of the IEEE Conference on Computer Vision and Pattern Recognition, pages 3559–3568, 2018. 1, 2, 5, 8
- [16] V. Lepetit, F. Moreno-Noguer, and P. Fua. Epnp: An accurate o (n) solution to the pnp problem. *International journal of computer vision*, 81(2):155, 2009.
- [17] X. Liang, X. Shen, D. Xiang, J. Feng, L. Lin, and S. Yan. Semantic object parsing with local-global long short-term memory. In *Proceedings of the IEEE Conference on Computer Vision and Pattern Recognition*, pages 3185–3193, 2016. 2
- [18] Y.-L. Lin, V. I. Morariu, W. Hsu, and L. S. Davis. Jointly optimizing 3d model fitting and fine-grained classification. In *European Conference on Computer Vision*, pages 466– 480. Springer, 2014.
- [19] S. Liu, J. Shi, J. Liang, and M.-H. Yang. Face parsing via recurrent propagation. arXiv preprint arXiv:1708.01936, 2017.
 1. 2
- [20] X. Liu, N.-G. Cho, P. Wang, X. Lian, J. Mao, A. Yuille, and S.-W. Lee. PASCAL Semantic Part: Dataset and Benchmark. http://www.stat.ucla.edu/~xiaochen. lian/paspart_challenge/index.html, 2014. [Online; accessed 16-November-2018]. 2
- [21] M. M. Loper and M. J. Black. Opendr: An approximate differentiable renderer. In *European Conference on Computer Vision*, pages 154–169. Springer, 2014.
- [22] A. Mousavian, D. Anguelov, J. Flynn, and J. Košecká. 3d bounding box estimation using deep learning and geometry. In *Computer Vision and Pattern Recognition (CVPR)*, 2017 IEEE Conference on, pages 5632–5640. IEEE, 2017. 2, 5, 7, 8
- [23] G. Pavlakos, X. Zhou, A. Chan, K. G. Derpanis, and K. Daniilidis. 6-dof object pose from semantic keypoints. In Robotics and Automation (ICRA), 2017 IEEE International Conference on, pages 2011–2018. IEEE, 2017. 1, 2
- [24] P. Poirson, P. Ammirato, C.-Y. Fu, W. Liu, J. Kosecka, and A. C. Berg. Fast single shot detection and pose estimation. In 3D Vision (3DV), 2016 Fourth International Conference on, pages 676–684. IEEE, 2016. 2
- [25] S. R. Richter, Z. Hayder, and V. Koltun. Playing for benchmarks. In *International Conference on Computer Vision* (ICCV), 2017. 3
- [26] G. Ros, L. Sellart, J. Materzynska, D. Vazquez, and A. M. Lopez. The synthia dataset: A large collection of synthetic images for semantic segmentation of urban scenes. In *Proceedings of the IEEE conference on computer vision and pattern recognition*, pages 3234–3243, 2016. 3
- [27] B. M. Smith, L. Zhang, J. Brandt, Z. Lin, and J. Yang. Exemplar-based face parsing. In *Proceedings of the IEEE Conference on Computer Vision and Pattern Recognition*, pages 3484–3491, 2013. 1, 2
- [28] Y. Song, X. Chen, J. Li, and Q. Zhao. Embedding 3d geometric features for rigid object part segmentation. In Proceedings of the IEEE International Conference on Computer Vision, pages 580–588, 2017. 2

- [29] O. Sorkine and M. Alexa. As-rigid-as-possible surface modeling. In *Symposium on Geometry processing*, volume 4, pages 109–116, 2007. 3
- [30] H. Su, C. R. Qi, Y. Li, and L. J. Guibas. Render for cnn: Viewpoint estimation in images using cnns trained with rendered 3d model views. In *Proceedings of the IEEE International Conference on Computer Vision*, pages 2686–2694, 2015. 2
- [31] R. W. Sumner, J. Schmid, and M. Pauly. Embedded deformation for shape manipulation. In ACM Transactions on Graphics (TOG), volume 26, page 80. ACM, 2007. 3
- [32] J. Tremblay, A. Prakash, D. Acuna, M. Brophy, V. Jampani, C. Anil, T. To, E. Cameracci, S. Boochoon, and S. Birchfield. Training deep networks with synthetic data: Bridging the reality gap by domain randomization. Proceedings of the IEEE Conference on Computer Vision and Pattern Recognition Workshop on Autinomous Driving, 2018. 4
- [33] G. Varol, J. Romero, X. Martin, N. Mahmood, M. J. Black, I. Laptev, and C. Schmid. Learning from synthetic humans. In 2017 IEEE Conference on Computer Vision and Pattern Recognition (CVPR 2017), pages 4627–4635. IEEE, 2017. 1, 2
- [34] P. Wang, X. Shen, Z. Lin, S. Cohen, B. Price, and A. L. Yuille. Joint object and part segmentation using deep learned potentials. In *Proceedings of the IEEE International Conference on Computer Vision*, pages 1573–1581, 2015. 1, 2
- [35] Y. Wang, X. Tan, Y. Yang, X. Liu, E. Ding, F. Zhou, and L. S. Davis. 3d pose estimation for fine-grained object categories. arXiv preprint arXiv:1806.04314, 2018. 1
- [36] Z. Wu, C. Shen, and A. v. d. Hengel. Wider or deeper: Revisiting the resnet model for visual recognition. arXiv preprint arXiv:1611.10080, 2016. 4, 5
- [37] Y. Xiang, W. Choi, Y. Lin, and S. Savarese. Data-driven 3d voxel patterns for object category recognition. In *Proceedings of the IEEE Conference on Computer Vision and Pattern Recognition*, pages 1903–1911, 2015. 2
- [38] L. Yang, P. Luo, C. Change Loy, and X. Tang. A large-scale car dataset for fine-grained categorization and verification. In *Proceedings of the IEEE Conference on Computer Vision and Pattern Recognition*, pages 3973–3981, 2015. 1
- [39] X. Zhou, M. Zhu, S. Leonardos, and K. Daniilidis. Sparse representation for 3d shape estimation: A convex relaxation approach. *IEEE transactions on pattern analysis and machine intelligence*, 39(8):1648–1661, 2017. 1, 2
- [40] M. Zhu, X. Zhou, and K. Daniilidis. Single image pop-up from discriminatively learned parts. In *Proceedings of the IEEE International Conference on Computer Vision*, pages 927–935, 2015. 2

Supplemental Material

Qichuan Geng, Feixiang Lu, Xinyu Huang, Sen Wang Xinjing Cheng, Zhong Zhou, and Ruigang Yang

A. Estimation of Orientation

In order to achieve a fair comparison, we adopted a third-party 3D-RCNN implementation and further implemented the Deep3DBox. We first trained and evaluated the Deep3DBox on the Kitti dataset to verify that the performance is similar to the original performance. For instance, given ground truth 2D detections of bounding boxes, the AOS values for Deep3DBox are 99.86%, 96.94%, and 93.43% for easy, moderate, and hard cases respectively in the Kitti Dataset. Then, we trained and evaluated the networks on the ApolloScape dataset. In order to factor out the performance of 2D detector, we fixed the detections of 2D bounding boxes with 79.58% AP for detection based on a third-party Mask-RCNN implementation [1].

Table 1 shows the comparison of average orientation similarities from three networks. We only show the results for the azimuth angle as elevation and tilt angles are not estimated by Deep3DBox. Based on the same dataset and the same 2D detections, our approach outperforms Deep3DBox and 3D-RCNN by 4.17% and 3.08% on AOS. We further notice that existing approaches could be greatly affected by the performance of 2D detector. When more occlusions or truncations present, cropped global features could cause more ambiguities. Our pose and shape network could reduce this kind of ambiguities by using part-level features and 3D losses.

Table 1. Evaluation of car orientation using average orientation similarity (AOS) and orientation score (OS). Average precision (AP) for detection is 79.58%. All networks are trained and evaluated on the ApolloScape dataset.

	Deep3DBox	3D-RCNN	Our Network
AOS	72.61%	73.70%	76.78%
OS	91.24%	92.61%	96.48%

B. Semantic Parts

In this section, we provide a complete list of 70 semantic parts annotated in the 3D dataset. There are four major categories, light, body, window, and other parts. Table 2 shows the details of these parts.

Table 2. A complete list of 70 semantic parts.

	1
category	class
light	left headlight, left fog light, right head-
	light, right fog light, left tail light, right tail
	light
body	front left door, front right door, rear left
	door, rear right door, left side sill, right side
	sill, roof, hood, tailgate, front bumper, rear
	bumper, fuel door, left mirror, right mir-
	ror, front left fender, front right fender, rear
	left fender, rear right fender, front left door
	handle, front right door handle, rear left
	door handle, rear right door handle, front car logo, rear car logo, A/B pillar, chassis,
	grilles
window	windscreen wiper, rear window wiper,
***************************************	windscreen, rear window, front left door
	window, rear left side window, rear left
	quarter glass, rear right side window, front
	right door window, rear right quarter glass,
	rear left quarter glass on door, rear right
	quarter glass on door
others	front left wheel/tire, rear left wheel/tire,
	front right wheel/tire, rear right wheel/tire,
	antenna, exhaust(pipe), spare tire, roof
	rack/taxi display, left side step pedal, right
	side step pedal, rear left fender II, rear left
	door II, rear left spoiler, rear right spoiler,
	rear right fender II, rear right door II, rear
	heat sink, left A pillar II, right A pillar II

References

[1] An MXNet Implementation of Mask-RCNN. https://github.com/TuSimple/mx-maskrcnn, 2017. [Online; accessed 21-November-2018].